Geochemical Perspectives Letters



# Fate of organic compounds during transformation of ferrihydrite in iron formations

**S. Jelavić, A.C. Mitchell, K.K. Sand**

## Supplementary Information

The Supplementary Information includes:

- Tip Functionalisation
- Cleaning of Hematite Substrate
- Dynamic Force Spectroscopy (DFS)
- The effect of temperature on $\Delta G_{bu}$
- Estimating the adsorption capacity of ferrihydrite for glycerol
- X-ray Diffraction (XRD)
- Estimation of the Specific Surface Area (SSA)
- Supplementary Information References

### *Tip Functionalisation*

Tips were cleaned in the UV/ozone chamber for 20 min and functionalized by placing them in 1 mM ethanol (anhydrous, ≥99.5 %, Sigma-Aldrich) solution of 11-mercaptoundecanoic acid (HS-$(CH_2)_{10}$COOH, 95 %, Sigma-Aldrich) with 10 wt.% of anhydrous acetic acid (≥99 %, Sigma Aldrich) for preparation of carboxylic tips, 11-mercaptoundecylphosphoric acid (HS-$(CH_2)_{11}H_2PO_4$, 90 %; Sigma-Aldrich) for phosphate tips or 11-mercapto-1-undecanol (HS-$(CH_2)_{11}$OH, 99 %, Sigma-Aldrich) for preparation of alcohol tips. Tips were left in a thiol solution overnight to form a self-assembled monolayer (SAM) where –COOH, –OH or $–OPO_3H_2$ headgroups point away from the AFM probe and into the solution. Excess thiols were rinsed by keeping the tips in ethanol (anhydrous, ≥99.5 %, Sigma-Aldrich) for 20 min immediately prior to their use.

## *Cleaning of Hematite Substrate*

We washed the hematite substrate in 1 M NaOH (≥98 %, Sigma Aldrich) maintained at 60 ºC for 1 hour. Subsequently, we sonicated the solution for 20 minutes to remove the particulate contamination, washed the substrates under flowing MiliQ (ultradeionised water, resistivity >18.2 MΩcm), dried it with $N_2$ and placed in an UV/ozone chamber for 30 min to remove the adventitious carbon (organic compounds adsorbed from air or solution). A fully hydrated {0001} hematite surface, as encountered in aqueous solutions, predominantly consists of hydroxylated terminal Fe and O in similar proportions (~50:50) (Trainor *et al*., 2004; Tanwar *et al*., 2009*)*, where the hydroxyls are mainly doubly coordinated (Barrón and Torrent, 1996; Eggleston *et al*., 2003).

## *Dynamic Force Spectroscopy (DFS)*

Dynamic Forces Spectroscopy (DFS) is a technique of Atomic Force Microscopy (AFM) that relies on formation of a bond between the AFM probe and the mineral surface (Fig. 1a). Here, we have decorated the probe with organic functional groups. Once the bond between the molecules at the functionalized probe and the surface is formed, the bond is forcefully broken and the rupture force measured as a function of distance between the probe and the surface. One cycle of the tip approaching, dwelling and retracting from the surface is called a force curve (Fig. 1b). A discontinuity in the retraction path of the force curve represents the rupture of a bond. The rupture force is not an intrinsic property of the bond but depends on the velocity by which the tip and the mineral surface are separated i.e. the rupture forces increase as the retraction velocity increases (Evans and Ritchie, 1997).

The retraction velocities are recalculated to loading rates, $r$, defined as $r=kv$, where $k$ represents the spring constant of the AFM cantilever and $v$ represents the retraction velocity of the tip. The plot of recorded rupture forces as a function of loading rate is called a force spectrum (*e.g*., Fig. 2) that is defined by the near-equilibrium and kinetic regimes. In the near-equilibrium regime, the loading rate is so slow that the rates of bond forming and breaking are equal. This regime is characterised by rupture forces being independent of the loading rate, *i.e.* the force spectrum curve is subparallel to the *y*-axis. In the kinetic regime, the rate of bond breaking is faster than the rate of bond forming. This regime is characterised by rupture forces increasing exponentially with the increase in loading rate.

We then fit these two regimes to a multibond model (Friddle *et al*., 2012) defined as:

$$\langle f \rangle \cong f_{eq} + f_{\beta}^{app} \ln\left(1 + e^{-\gamma} R(f_{eq})\right), \quad \text{Eq. S-1}$$

$$f_{\beta}^{app} = N \frac{k_B T}{x_t}, \quad \text{Eq. S-2}$$

$$R(f_{eq}/N) = \frac{r}{f_{\beta}^{app} k_{off} f_{eq}}, \quad \text{Eq. S-3}$$

where $f$ represents the rupture force, $f_{eq}$ the equilibrium rupture force, $\gamma$ the Euler constant, $N$ the number of interacting bonds, $k_B$ the Boltzmann constant, $T$ the temperature, $x_t$ the distance between the energy minimum of a bound and the transition state and $k_{off}$ represents the intrinsic kinetic unbinding (off) rate. $f_{eq}$, $x_t$ and $k_{off}$

are binding parameters that define the energy landscape of a bond. The bond parameters determined in this study are given in Table S-1.

**Table S-1** Bond parameters.

| | Hematite – $HPO_4^-$ | Hematite – $COO^-$ | Hematite – OH |
|---|---|---|---|
| $x_t$ (Å) | 0.4 ± 0.3 | 0.40 ± 0.04 | 0.10 ± 0.04 |
| $k_{off}$ ($s^{-1}$) | 241 ± 352 | 1934 ± 570 | 1351 ± 1360 |
| $f_{eq}$ (pN) | 104 ± 18 | 83 ± 8 | 597 ± 18 |

* uncertainty expressed as a standard deviation

Usually, not one but many bonds form between the tip and the surface, thus the recorded rupture forces represent breaking of an undefined ensemble of bonds, which complicates comparison among tips functionalised with different functional groups. However, this problem can be circumvented by comparing the Gibbs free energy of binding ($\Delta G_{bu}$) derived from bond parameters. $f_{eq}$ and $x_t$ are used to calculate $\Delta G_{bu}$ through (Friddle *et al.*, 2012):

$$\Delta G_{bu} = k_B T \ln \frac{f_{eq} x_t}{k_B T} + f_{eq} x_t + k_B T. \qquad \text{Eq. S-4}$$

The bond strength between organic compounds and mineral surfaces depends on the composition of the surrounding solution, in particular the pH and the ionic strength. We have conducted our DFS experiments at pH=5.5 and at 10 mM NaCl. Our pH is for ~1.5 unit lower than the current estimates for Precambrian seawater (Halevy and Bachan, 2017; Krissansen-Totton *et al.*, 2018). However, we chose this pH because the surface potential of hematite {0001} is mostly neutral and the zeta potential is slightly positive (Lützenkirchen *et al.*, 2013), which resembles the surface properties of particulate hematite at circumneutral conditions (Kosmulski, 2009) present during the Precambrian. We used a solution concentration of 10 mM instead of higher concentration typical for seawater to maximize the interactions (Newcomb *et al.*, 2017). We chose not to work with solution similar to seawater because we wanted to avoid issues with high activities of divalent cations.

For all DFS measurements, the spring constant of the probe was calculated using a thermal calibration method (Hutter and Bechhoefer, 1993). Our $\Delta G_{bu}$ are comparable to values between goethite and $COO^-$ (1.0 ± 0.6 kT), and goethite and $PO_3^-$ (1.6 ± 0.9 kT ) obtained at similar solution conditions (Newcomb *et al.*, 2017).

## *The Effect of Temperature on $\Delta G_{bu}$*

From van't Hoff's equation (Denbigh, 1981), it follows that for exothermic reactions, $\Delta G_{bu}$ decreases with increasing temperature. This implies that at the temperatures such were common in Precambrian oceans, i.e. 50-85 °C (Knauth, 2005; Robert and Chaussidon, 2006; Garcia *et al.*, 2017), the binding between organic functional groups and iron (oxyhydr)oxides was weaker compared to binding at the temperature at which the DFS experiments were conducted. In addition, an increase in temperature results in a decrease in the point of zero charge of iron (oxyhydr)oxides (Rodda *et al.*, 1993) again suggesting weaker binding to carboxyl, phosphate and hydroxyl functional groups (Newcomb *et al.*, 2017) if the interactions are purely electrostatic (Sposito, 2004). Combined, the binding between organic functional groups and iron (oxyhydr)oxides was weaker in Precambrian oceans than at room temperature experiments implying even higher desorption of

organic compounds during mineral transformation than shown in our experiments. This reinforces our hypothesis that the organic compounds were largely absent from iron formations since their deposition.

## *Estimating the Adsorption Capacity of Ferrihydrite for Glycerol*

To estimate the adsorption capacity of ferrihydrite for glycerol, we conducted batch experiments. The samples were prepared in the same way as the samples for transformation experiments except they were not washed. After centrifugation, the supernatant was collected and the concentration of glycerol measured with spectrophotometry (Bondioli and Bella, 2005). In short, the glycerol was oxidised with sodium periodate ($NaIO_4$, Sigma Aldrich, ≥99.8 %) to formaldehyde ($CH_2O$), which was subsequently reacted with acetylacetone ($(CH_3)_2(CO)_2CH_2$, Merck, ≥99 %) in presence of ammonium acetate ($NH_4CH_3CO_2$) as a source of N to give highly absorptive complex (410 nm) 3,5-diacetyl-1,4-dihydrolutidine ($C_{11}H_{15}NO_2$). The absorption of the complex was measured using Thermo Scientific Multiskan Microplate Spectrophotometer. We prepared 7 standards (0.064, 0.036, 0.024, 0.018, 0.0135, 0.009 and 0.0045 $mgml^{-1}$) and a blank sample to calibrate the instrument. The samples were prepared in triplicates and the analysis of samples, standards and the blank were repeated twice to account for the instrumental uncertainty.

Figure S-1 shows the adsorption isotherm and the corresponding Freundlich fit to the data. Based on these results, we decided to conduct transformation experiments at glycerol concentration of 0.5 % which corresponds to the equilibrium concentration of ~ Ce= 1000 $mgL^{-1}$. We chose to do so to minimise the intermolecular interactions that do not influence the glycerol-ferrihydrite binding energy but would significantly decrease the transformation rates.

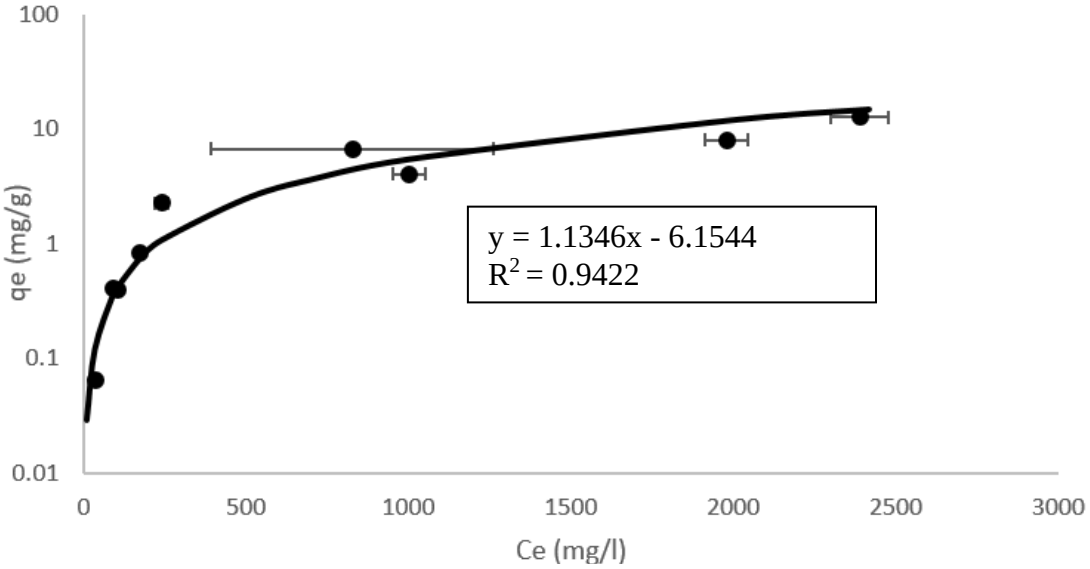


**Figure S-1** Adsorption isotherm of glycerol on ferrihydrite and the corresponding Freundlich fit. $q_e$ represents the mass of adsorbed glycerol per gram of ferrihydrite and $C_e$ represents the equilibrium concentration of glycerol in contact with ferrihdyrite. Insert represents the equation of the fit and the $R^2$ represents the coefficient of determination. Uncertainties are shown as standard deviations. The uncertainty for $q_e$ are smaller than the size of a symbol.

# *X-ray Diffraction (XRD)*

To maximise diffracted intensities from a small amount of material, the instrumental profile was set in such a way which resulted in the diameter of the incident X-rays being longer than the diameter of the zero background Si plate. This meant that there was some diffused scattering arising from the surrounding poly(methyl methacrylate) holder. To remove that diffused contribution, we have subtracted a diffractogram of a blank poly(methyl methacrylate) holder from each measured sample.

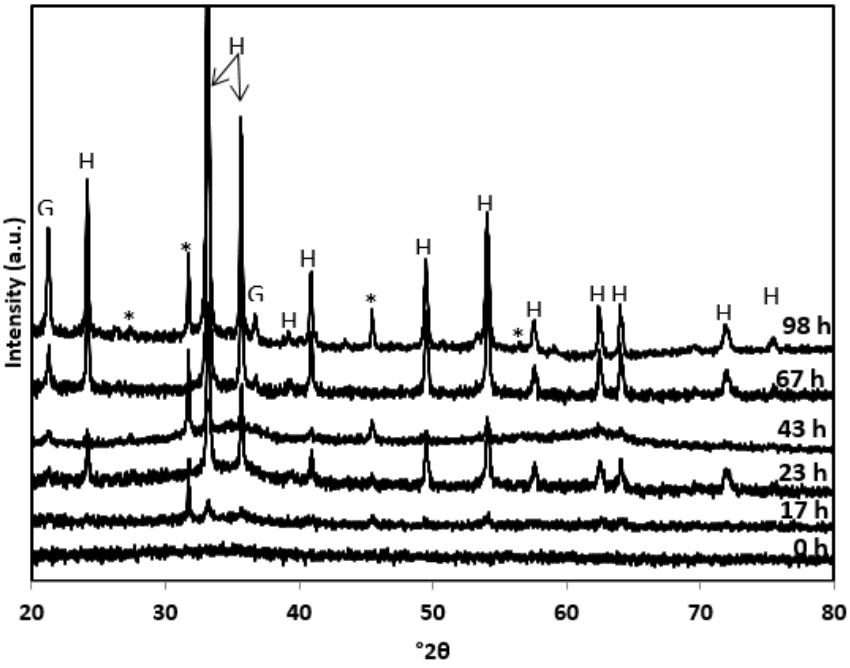


**Figure S-2** X-ray diffractograms for the succesive samples (0-98 h) obtained by aging ferrihydrite in 0.5 M NaCl solution at 90 °C. The diffractogram at 0 h was collected on a sample that was equilibrated overnight and analysed immediately. The diffractogram of the product obtained after 98 h of aging shows reflections of goethite (G), hematite (H) and halite (*). Halite is present in samples in which it was not possible to completely remove it by washing with MiliQ. Diffractograms are scaled along the *y*-axis for clarity.

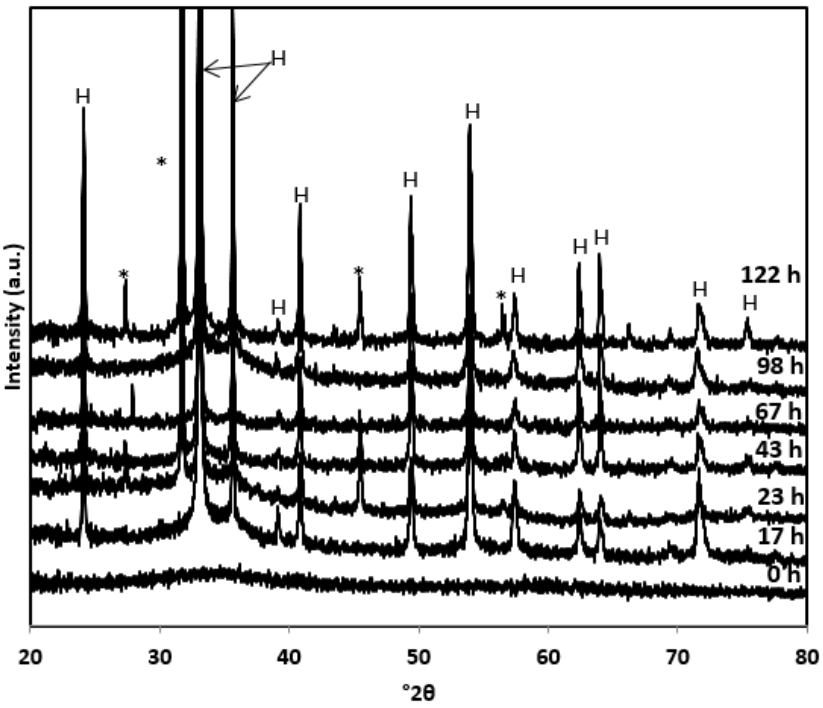


**Figure S-3** X-ray diffractograms for the succesive samples (0-120 h) obtained by aging ferrihydrite in 0.5 M NaCl solution at 90 °C in presence of glycerol. The diffractogram at 0 h was collected on a sample that was equilibrated overnight and analysed immediately. The only FeOx species present in the product after 120 h of aging is hematite (H). Halite is present in samples in which it was not possible to completely remove it by washing. Diffractograms are scaled along the *y*-axis for clarity.

## *Estimation of the Specific Surface Area (SSA)*

We estimated the SSA of the precursor ferrihydrite and produced hematite by assuming an ideal, non porous spherical shape of ferrihydrite particles and by taking an average of observed particle dimensions of hematite. Our TEM images are not of sufficient resolution to directly measure the diameter of ferrihydrite particles but we know that our precursor ferrihydrite is "2-line" (Figs. S-2 and S-3). The maximum observed size for 2-line ferrihydrite is 3 nm (Janney *et al.*, 2000) so we calculated the range of possible SSA's by taking:

$$\boldsymbol{SSA\ (ferrihydrite)} = \frac{\boldsymbol{6}}{\boldsymbol{\rho d}}, \qquad \text{Eq. S-5}$$

where $\rho$ represents the mass density of ferrihydrite taken as 3.8 gcm$^{-3}$ and $d$ represents the particle diameter (between 2-3 nm). This gave values of SSA for ferrihydrite between 526-790 m$^2$g$^{-1}$.

The SSA for hematite was estimated by taking:

$$\boldsymbol{SSA\ (hematite)} = \frac{\boldsymbol{2lw + 2lt + 2tw}}{\boldsymbol{\rho abc}}, \qquad \text{Eq. S-6}$$

where *l* represents the average of observed particle lengths, *w* represents the average of particle widths and *t* represents the assumed particle thickness. We took a minimum particle thickness to be 10 nm and maximum to be equal to the average of observed particle widths. This gave estimated SSA for hematite product in range of 11-46 $m^2g^{-1}$.

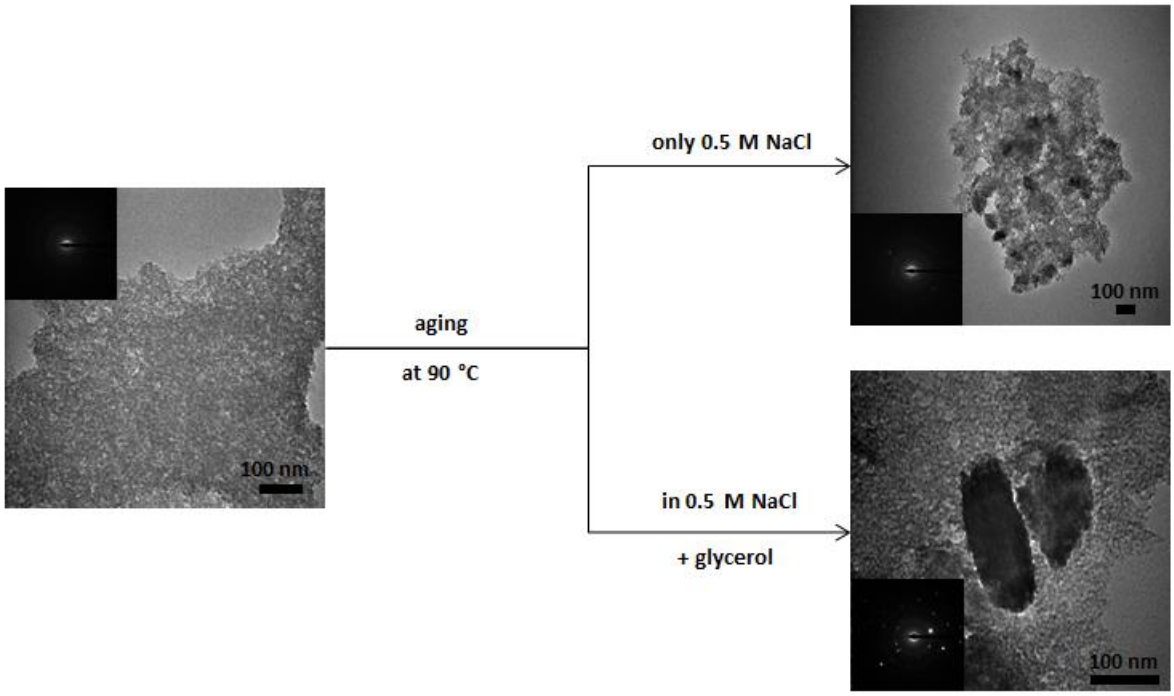


**Figure S-4** TEM images of ferrihydrite precursor (left), ferrihydrite aged in 0.5 M NaCl solution (upper right) and ferrihydrite aged in 0.5 M NaCl and 0.5 % glycerol.

## *Supplementary Information References*

Barrón, V., Torrent, J. (1996) Surface Hydroxyl Configuration of Various Crystal Faces of Hematite and Goethite. *Journal of Colloid and Interface Science* 177, 407–410.

Bondioli, P., Bella, L.D. (2005) An alternative spectrophotometric method for the determination of free glycerol in biodiesel. *European Journal of Lipid Science and Technology* 107, 153–157.

Denbigh, K.G. (1981) Equilibria of Reactions Involving Gases. In: *The Principles of Chemical Equilibrium: With Applications in Chemistry and Chemical Engineering*. Cambridge University Press, Cambridge, 133–181.

Eggleston, C.M., Stack, A.G., Rosso, K.M., Higgins, S.R., Bice, A.M., Boese, S.W., Pribyl, R.D., Nichols, J.J. (2003) The structure of hematite ($\alpha$-$Fe_2O_3$) (001) surfaces in aqueous media: scanning tunneling microscopy and resonant tunneling calculations of coexisting O and Fe terminations. *Geochimica et Cosmochimica Acta* 67, 985–1000.

Evans, E., Ritchie, K. (1997) Dynamic strength of molecular adhesion bonds. *Biophysical Journal* 72, 1541–1555.

Friddle, R.W., Noy, A., Yoreo, J.J.D. (2012) Interpreting the widespread nonlinear force spectra of intermolecular bonds. *Proceedings of the National Academy of Sciences* 109, 13573–13578.

Garcia, A.K., Schopf, J.W., Yokobori, S., Akanuma, S., Yamagishi, A. (2017) Reconstructed ancestral enzymes suggest long-term cooling of Earth's photic zone since the Archean. *Proceedings of the National Academy of Sciences* 114, 4619–4624.

Halevy, I., Bachan, A. (2017) The geologic history of seawater pH. *Science* 355, 1069–1071.

Hutter, J.L., Bechhoefer, J. (1993) Calibration of atomic-force microscope tips. *Review of Scientific Instruments* 64, 1868–1873.

Janney, D.E., Cowley, J.M., Buseck, P.R. (2000) Transmission Electron Microscopy of Synthetic 2- and 6-Line Ferrihydrite. *Clays and Clay Minerals* 48, 111–119.

Knauth, L.P. (2005) Temperature and salinity history of the Precambrian ocean: implications for the course of microbial evolution. *Palaeogeography, Palaeoclimatology, Palaeoecology*, Geobiology: Objectives, Concept, Perspectives 219, 53–69.

Kosmulski, M. (2009) *Surface Charging and Points of Zero Charge*. CRC Press, Boca Raton.

Krissansen-Totton, J., Arney, G.N., Catling, D.C. (2018) Constraining the climate and ocean pH of the early Earth with a geological carbon cycle model. *Proceedings of the National Academy of Sciences* 115, 4105–4110.

Lützenkirchen, J., Preočanin, T., Stipić, F., Heberling, F., Rosenqvist, J., Kallay, N. (2013) Surface potential at the hematite (001) crystal plane in aqueous environments and the effects of prolonged aging in water. *Geochimica et Cosmochimica Acta* 120, 479–486.

Newcomb, C.J., Qafoku, N.P., Grate, J.W., Bailey, V.L., Yoreo, J.J.D. (2017) Developing a molecular picture of soil organic matter–mineral interactions by quantifying organo–mineral binding. *Nature Communications* 8, 396.

Robert, F., Chaussidon, M. (2006) A palaeotemperature curve for the Precambrian oceans based on silicon isotopes in cherts. *Nature* 443, 969–972.

Rodda, D.P., Johnson, B.B., Wells, J.D. (1993) The Effect of Temperature and pH on the Adsorption of Copper (II), Lead (II), and Zinc (II) onto Goethite. *Journal of Colloid and Interface Science* 161, 57–62.

Sposito, G. (2004) *The Surface Chemistry of Natural Particles*. Oxford University Press, New York.

Tanwar, K.S., Petitto, S.C., Ghose, S.K., Eng, P.J., Trainor, T.P. (2009) Fe (II) adsorption on hematite (0001). *Geochimica et Cosmochimica Acta* 73, 4346–4365.

Trainor, T.P., Chaka, A.M., Eng, P.J., Newville, M., Waychunas, G.A., Catalano, J.G., Brown, G.E. (2004) Structure and reactivity of the hydrated hematite (0001) surface. *Surface Science* 573, 204–224.